






This article has been accepted for publication in Monthly Notices of the Royal Astronomical Society ©: 2021 The Authors. Published by Oxford University Press on behalf of the Royal Astronomical Society. All rights reserved.

SEAGLE – III: Towards resolving the mismatch in the dark-matter fraction in early-type galaxies between simulations and observations

Sampath Mukherjee ^{1,2}★, Léon V. E. Koopmans ¹★, Crescenzo Tortora ³, Matthieu Schaller ^{4,5}, R. Benton Metcalf ^{6,7}, Joop Schaye ⁵ and Georgios Vernardos ⁸

¹*Kapteyn Astronomical Institute, University of Groningen, PO Box 800, NL-9700 AV Groningen, the Netherlands*

²*STAR Institute, Quartier Agora, Allée du Six Août, 19c, B-4000 Liège, Belgium*

³*INAF – Osservatorio Astronomico di Capodimonte, Salita Moiariello 16, I-80131 Napoli, Italy*

⁴*Lorentz Institute for Theoretical Physics, Leiden University, PO Box 9506, NL-2300 RA Leiden, the Netherlands*

⁵*Leiden Observatory, Leiden University, PO Box 9513, NL-2300 RA Leiden, the Netherlands*

⁶*Dipartimento di Fisica e Astronomia, Università di Bologna, Via Gobetti 93/2, I-40129 Bologna, Italy*

⁷*INAF – Osservatorio di Astrofisica e Scienza dello Spazio di Bologna, Via Gobetti 93/3, I-40129 Bologna, Italy*

⁸*Institute of Physics, Laboratory of Astrophysique, École Polytechnique Fédérale de Lausanne (EPFL), Observatoire de Sauverny, CH-1290 Versoix, Switzerland*

Accepted 2021 October 12. Received 2021 September 4; in original form 2021 April 12

ABSTRACT

The central dark-matter fraction of galaxies is sensitive to feedback processes during galaxy formation. Strong gravitational lensing has been effective in the precise measurement of the dark-matter fraction inside massive early-type galaxies. Here, we compare the projected dark-matter fraction of early-type galaxies inferred from the SLACS (Sloan Lens ACS Survey) strong-lens survey with those obtained from the Evolution and Assembly of GaLaxies and their Environment (EAGLE), Illustris, and IllustrisTNG hydrodynamical simulations. Previous comparisons with some simulations revealed a large discrepancy, with considerably higher inferred dark-matter fractions – by factors of ≈ 2 – 3 – inside half of the effective radius in observed strong-lens galaxies as compared to simulated galaxies. Here, we report good agreement between EAGLE and SLACS for the dark-matter fractions inside both half of the effective radius and the effective radius as a function of the galaxy’s stellar mass, effective radius, and total mass-density slope. However, for IllustrisTNG and Illustris, the dark-matter fractions are lower than observed. This work consistently assumes a Chabrier initial mass function (IMF), which suggests that a different IMF (although not excluded) is not necessary to resolve this mismatch. The differences in the stellar feedback model between EAGLE and Illustris and IllustrisTNG are likely the dominant cause of the difference in their dark-matter fraction and density slope.

Key words: gravitational lensing: strong – methods: numerical – galaxies: elliptical and lenticular, cD – galaxies: evolution – galaxies: structure – dark matter.

1 INTRODUCTION

The study of massive early-type galaxies (ETGs) has been of central interest in galaxy evolution and cosmological studies. ETGs are believed to be the end product of hierarchical galaxy formation (e.g. Toomre & Toomre 1972; Cole et al. 2000). The determination of the distribution of baryonic and dark matter within these galaxies is a key step in addressing open questions in galaxy formation and evolution (e.g. Cappellari et al. 2006; Koopmans et al. 2009; Auger et al. 2010b; Napolitano, Romanowsky & Tortora 2010; Tortora et al. 2012, 2018; Lovell et al. 2018). One of the still not well-understood issues originating from the gravitational interplay between baryonic and dark matter during galaxy formation results in the so-called bulge–halo conspiracy referring to the total mass distribution following a nearly isothermal profile while the baryons and dark matter, individually, do not (Cappellari et al. 2006; Treu

et al. 2006; Humphrey & Buote 2010; Thomas et al. 2011; Tortora et al. 2014). The evidence for this has been reported in strong and weak lensing (Treu & Koopmans 2004; Gavazzi et al. 2007; Auger et al. 2010b) and in stellar-dynamics studies (Dutton & Treu 2014; Tortora et al. 2014; Li et al. 2019). However, a particular choice for the stellar initial mass function (IMF) is often assumed because it is usually ill-determined. Furthermore, two parameters have often been used to quantify the distribution of dark matter: the dark-matter fraction within a given radius (f_{DM}) and the logarithmic slope (γ) of the total density profile. To correctly infer f_{DM} from simulations, one therefore additionally requires the simulations to yield $\gamma \approx 2$ – the isothermal case – for the combination of baryonic and dark matter, both of which are individually non-isothermal (Auger et al. 2010b; Tortora et al. 2014).

Until recently, cosmological hydrodynamic simulations have been unable to simultaneously match both the observed f_{DM} and γ distributions. The isothermal density slopes can be reproduced in simulations by having no or weak feedback, but this leads to an overestimated galaxy formation efficiency and an underestimated

* E-mail: sampath@astro.rug.nl (SM); koopmans@astro.rug.nl (LK)

dark-matter fraction (Duffy et al. 2010). Conversely, reproducing the observed dark-matter fraction requires strong feedback, but predicts total density slopes that are shallower (smaller γ) than isothermal (Dubois et al. 2013).

For example, Xu et al. (2017) studied elliptical galaxies from the Illustris hydrodynamic simulations (Vogelsberger et al. 2014), finding lower dark-matter fractions and steeper density slopes inside half of an effective radius than those observed in elliptical galaxies (Auger et al. 2009, 2010a). A similar trend is found in IllustrisTNG (see the middle panel of fig. 9 in Wang et al. 2019). Remus et al. (2017) found that f_{DM} in the MAGNETICUM simulations is lower than observed.¹ These mismatches point to either an inadequacy in the theoretical model or systematic biases in the observational methods. Having found lower f_{DM} values in IllustrisTNG than in Sloan Lens ACS Survey (SLACS), Wang et al. (2019) suggest that a Salpeter IMF, as favoured by strong lensing observations, would result in lower central dark-matter fractions for observed galaxies and can mitigate the apparent mismatch of f_{DM} though we note that IllustrisTNG uses a Chabrier IMF.

To investigate whether this discrepancy between observations and simulations is the result of galaxy formation processes, we use the publicly available Evolution and Assembly of GaLaxies and their Environment (EAGLE) hydro simulations (Crain et al. 2015; Schaye et al. 2015) to perform a detailed comparison of the central dark-matter fractions, evaluated at both one-half effective radius ($R_{\text{eff}}/2$) and one effective radius (R_{eff}) from simulations and strong gravitational lensing observations of the SLACS (Bolton et al. 2006; Koopmans et al. 2006, 2009; Auger et al. 2010a, b; Shu et al. 2017). We also make use of the publicly available Illustris and IllustrisTNG simulations (Vogelsberger et al. 2014; Wang et al. 2019) that have different implementations of feedback than EAGLE.

This paper is structured as follows: In Section 2, we summarize the EAGLE, Illustris, and IllustrisTNG galaxy formation simulations and the relevant codes that we use in our analyses. Section 3 describes the methodology used to calculate f_{DM} . In Section 4, we discuss the dark-matter fractions obtained from simulations and compare them with SLACS galaxies and also with other simulations. The implications of our results for galaxy formation are discussed and summarized in Section 5. The values of the cosmological parameters are $\Omega_{\Lambda} = 0.693$, $\Omega_{\text{b}} = 0.048\,2519$, $\Omega_{\text{m}} = 0.307$, $h = H_0/(100 \text{ km s}^{-1} \text{ Mpc}^{-1}) = 0.6777$, and $\sigma_8 = 0.8288$. These are taken from the Planck satellite data release (Planck Collaboration XVI 2014), in accordance with the EAGLE, and IllustrisTNG simulations. Illustris, on the other hand, uses slightly different cosmological parameters, but previous analyses (Genel et al. 2018; Pillepich et al. 2018) have shown that these differences between Illustris and IllustrisTNG have negligible effects on the quantities explored in this work.

2 THE EAGLE, ILLUSTRIS, AND TNG SIMULATIONS

Here, we make use of the main Reference 100 cMpc of EAGLE, Illustris (107 cMpc), and IllustrisTNG (110 cMpc) models. EAGLE² is a suite of hydrodynamical simulations of the formation of galaxies and other astronomical systems in a Λ CDM universe (Crain et al.

2015; Schaye et al. 2015; McAlpine et al. 2016). The simulations use a modified SPH (Smoothed Particle Hydrodynamics) version of GADGET 3 (Springel 2005), with a gravitational softening length of 2.66 comoving kpc (ckpc), limited to a maximum physical scale of 0.7 proper kpc (pkpc). The initial particle masses for baryons and dark matter are $m_{\text{b}} = 1.8 \times 10^6 M_{\odot}$ and $m_{\text{dm}} = 9.7 \times 10^6 M_{\odot}$, respectively. The prescriptions for stellar and active galactic nucleus (AGN) feedback were calibrated to broadly reproduce the observed present-day galaxy stellar mass function, disc sizes, and the relation between black hole and galaxy masses. The subgrid physics includes radiative cooling (Wiersma, Schaye & Smith 2009a), star formation (Schaye & Dalla Vecchia 2008), stellar mass-loss (Wiersma et al. 2009b), thermal energy feedback from star formation (Dalla Vecchia & Schaye 2012), black hole accretion, and AGN feedback (Rosas-Guevara et al. 2015; Schaye et al. 2015). The resulting galaxies are in broad agreement with observed properties such as the star formation rate, passive galaxy fraction, Tully–Fisher relation and colours (Schaye et al. 2015; Trayford et al. 2015), and rotation curves (Schaller et al. 2015).

Illustris³ and IllustrisTNG⁴ use the AREPO code (Springel 2010) that employs a tree-particle-mesh algorithm to solve Poisson’s equation for gravity and a second-order accurate finite-volume Godunov scheme on a moving, unstructured Voronoi mesh for the equations of ideal magnetohydrodynamics. IllustrisTNG (Nelson et al. 2019) builds upon the Illustris simulation (Vogelsberger et al. 2014; Xu et al. 2017) and improves upon Illustris by (a) extending the mass range of the simulated galaxies and haloes, and (b) adopting improved numerical and astrophysical modelling relative to Illustris (Pillepich et al. 2018). In this work, we use the IllustrisTNG simulation box with a side length of 110.7 cMpc having $m_{\text{b}} = 1.4 \times 10^6 M_{\odot}$ and $m_{\text{dm}} = 7.5 \times 10^6 M_{\odot}$. The Illustris run also has a side length of 106.5 cMpc and has $m_{\text{dm}} = 6.26 \times 10^6 M_{\odot}$ and $m_{\text{b}} = 1.26 \times 10^6 M_{\odot}$, resolving gravitational dynamics down to a physical scale of 0.710 pkpc. IllustrisTNG reproduces the galaxy stellar mass fraction and, similar to EAGLE, has an overall agreement with observations (Genel et al. 2018; Wang et al. 2019).

The simulations from EAGLE and the entire Illustris family assume a Chabrier stellar IMF (Chabrier 2003). Thus, we can compare the dark-matter fractions for all three simulations on an equal footing without having to make any adjustments to their properties.

3 ASSUMPTIONS AND DATA EXTRACTION

In this section, we discuss important assumptions pertaining to the stellar IMF and our analysis methodology.

3.1 The stellar IMF

Currently, most observational and theoretical studies of the stellar mass in galaxies rely on assumptions about the stellar IMF that in turn determines the stellar mass per unit luminosity. Auger et al. (2010b) found that differences in the stellar-population properties (e.g. age, metallicity, extinction, and star formation history) of very massive ETGs in the SLACS sample are not sufficient to account for the broad trends in their inferred total mass-to-light ratio values as a function of galaxy mass, for a non-varying (i.e. for a universal)

¹Remus et al. (2017) compared $f_{\text{DM}}(< R_{\text{eff}})$ from MAGNETICUM to $f_{\text{DM}}(< R_{\text{eff}}/2)$ in SLACS. Although not correct, comparing at the same radius would not resolve the discrepancy as shown by Wang et al. (2019).

²<http://icc.dur.ac.uk/Eagle/>

³<https://www.illustris-project.org/>

⁴<https://www.tng-project.org/>

IMF. Thus, Auger et al. (2010b) concluded that the total mass-to-light ratio in SLACS lens galaxies increases with their total stellar mass, most likely as a result of an increasing dark-matter fraction (see also Cappellari et al. 2006; Tortora et al. 2009; Thomas et al. 2011), although the stellar IMF itself cannot be determined from these data. Hence, the analyses of SLACS lens galaxies were done for both a Chabrier (2003) IMF and a Salpeter (1955) IMF. In this paper, we assume a Chabrier IMF for SLACS and compare with the results from EAGLE, Illustris, and IllustrisTNG where this IMF is also assumed. We refer the interested readers to Barber, Crain & Schaye (2018) for EAGLE simulations with variable IMFs.

3.2 Stellar and dark-matter masses, and effective radii

We select galaxies from the simulations based on their stellar mass and produce dark matter, stellar, and gas surface mass density maps, using the SEAGLE pipeline (Mukherjee et al. 2018, 2019, hereafter M18 and M19, respectively), which incorporates the GLAMER (Metcalf & Petkova 2014; Petkova, Metcalf & Giocoli 2014) ray-tracing code and the parametric lens-modelling code LENSED (Tessore, Bellagamba & Metcalf 2016; Bellagamba, Tessore & Metcalf 2017). We infer all quantities in this paper directly from these mass maps, by-passing the lens simulations and modelling steps, which we have shown in M18 and M19 to yield very similar results. We set a high total galaxy stellar-mass threshold of $>10^{11} M_{\odot}$ taken from the simulation catalogues, and excise outliers based on extreme values of their effective radius (see M18, and table 2 of M19). As in M18 and M19, we assume that the lens redshift is fixed at $z = 0.271$ for all mock lenses, typical for median SLACS lens redshifts. We expect evolutionary effects to be small compared to the large differences and scatter that are observed between these quantities (discussed further in M18 and M19, and below).

After extracting the particles of an individual galaxy, we project each galaxy along its three simulation coordinate axes, producing associated projected mass maps (M18). The effective radius, unlike in the observations, is not derived from the simulated galaxy brightness distribution via model fitting (e.g. with a Sérsic profile), but directly inferred from the simulated stellar mass profiles as the radius enclosing one-half of the total projected stellar mass. Similarly, the stellar and total masses are derived directly from the mass maps. We use the projected half stellar mass radius as a proxy for the stellar-light effective radius (i.e. R_{eff}) for each projected mass map. We finally calculate the central projected dark-matter fractions within half of the effective radius, $f_{\text{DM}}(< 0.5R_{\text{eff}})$ for all the EAGLE ETGs, following the definition in Tortora et al. (2009) and Auger et al. (2010b):

$$f_{\text{DM}} \equiv 1 - \frac{M_{*}(\beta R_{\text{eff}})}{M_{\text{T}}(\beta R_{\text{eff}})} \quad \text{with } \beta = 0.5 \text{ or } 1.0, \quad (1)$$

where $M_{*}(\beta R_{\text{eff}})$ is the projected stellar mass within βR_{eff} and $M_{\text{T}}(\beta R_{\text{eff}})$ is the total projected mass within βR_{eff} .

Because SLACS (Auger et al. 2010b) does not list dark-matter fractions within R_{eff} , we use the following equation to obtain it:

$$f_{\text{DM}}(< R_{\text{eff}}) \equiv 1 - \frac{1/2 M_{*}}{2 M_{R_{\text{eff}}/2}}, \quad (2)$$

where $M_{R_{\text{eff}}/2}$ is the total projected mass within $R_{\text{eff}}/2$ and M_{*} is the total projected stellar mass. The total mass within R_{eff} is then twice that within $R_{\text{eff}}/2$, assuming an isothermal model on average. The intrinsic scatter on the assumed mass-density slope is typically less than 10 per cent (Koopmans et al. 2009) and this simple extrapolation is assumed to be sufficiently accurate.

For IllustrisTNG, we use a combination of their publicly available data base⁵ and Wang et al. (2019). We obtain the effective radii and dark-matter fractions from the public data base (slight differences in fig. 1 is due to manual extraction of data from Wang et al. 2019). For slopes and dark-matter fractions within $R_{\text{eff}}/2$, we make use of results presented in Wang et al. (2019). We note that Xu et al. (2017) also present the dark-matter fraction at $R_{\text{eff}}/2$ and R_{eff} (see their fig. 11) and the M_{*} – R_{eff} relation from the Illustris simulations. For both Illustris and IllustrisTNG, we use the data for redshift $z = 0.3$, close to the redshift of $z = 0.271$ used in this work. No additional adjustments for cosmology are required because the cosmological parameters and IMF are almost identical for the three simulations used here.

4 RESULTS

In this section, we present the results obtained from our comparisons between observed and simulated galaxies, focusing particularly on dark-matter fractions within one half and one effective radius.

4.1 Dark-matter fractions inside $R_{\text{eff}}/2$

The mass distribution within half of the effective radius ($R_{\text{eff}}/2$) was chosen for SLACS galaxies (Koopmans et al. 2006; Auger et al. 2010a, b; Barnabè et al. 2011) because it is close to the average Einstein radius and therefore leads to smaller errors when interpolating or extrapolating the mass models from the Einstein radius to this reference radius than is the case for R_{eff} (see fig. 7 in Auger et al. 2010b). Moreover, the mass-density profile is sensitive to the scale over which it is modelled and might not represent the profile near the Einstein radius (e.g. Xu et al. 2017). Despite this, only one recent study of hydrodynamic simulations examined $f_{\text{DM}}(< 0.5R_{\text{eff}})$ (Xu et al. 2017; see fig. 11 therein).

4.1.1 Comparing SLACS, EAGLE, and Illustris(TNG)

Fig. 1 shows the trends of $f_{\text{DM}}(< 0.5R_{\text{eff}})$ (top row) and $f_{\text{DM}}(< R_{\text{eff}})$ (bottom row) against two different observables (M_{*} and R_{eff}) in the left and right columns, respectively, for galaxies from EAGLE at $z_1 = 0.271$, Illustris and IllustrisTNG (both at $z_1 = 0.3$), and SLACS. We find that the $f_{\text{DM}}(< 0.5R_{\text{eff}})$ values for SLACS and EAGLE Ref-100 are comparable, having values in the range of 0.5–0.7, whereas there is a clear mismatch with Illustris and IllustrisTNG (top left panel in Fig. 1).

When we plot $f_{\text{DM}}(< 0.5R_{\text{eff}})$ against R_{eff} , instead of against stellar mass, we find a tighter correlation for both EAGLE Ref-100 and IllustrisTNG (top right panel of Fig. 1). A tighter correlation between $f_{\text{DM}}(< 0.5R_{\text{eff}})$ and R_{eff} , rather than with M_{*} , was earlier reported for SLACS (Auger et al. 2010b). A correlation is expected in part because a larger R_{eff} encloses a larger portion of a galaxy’s dark-matter halo (e.g. Tortora et al. 2012, 2018; Remus et al. 2017; Xu et al. 2017). While EAGLE is in good agreement with the data, Illustris and IllustrisTNG predict dark-matter fractions within half of an effective radius that are appreciably lower than those for SLACS, or the effective radius needs to be much larger for a given f_{DM} value. The central DM fraction values $f_{\text{DM}}(< 0.5R_{\text{eff}})$ found in the Illustris and IllustrisTNG simulations thus differ sharply from SLACS, at fixed stellar mass (top panels in Fig. 1). In agreement with our results, Xu et al. (2017) calculated $f_{\text{DM}}(< 0.5R_{\text{eff}})$ and $f_{\text{DM}}(< R_{\text{eff}})$

⁵<https://www.tng-project.org/data/>

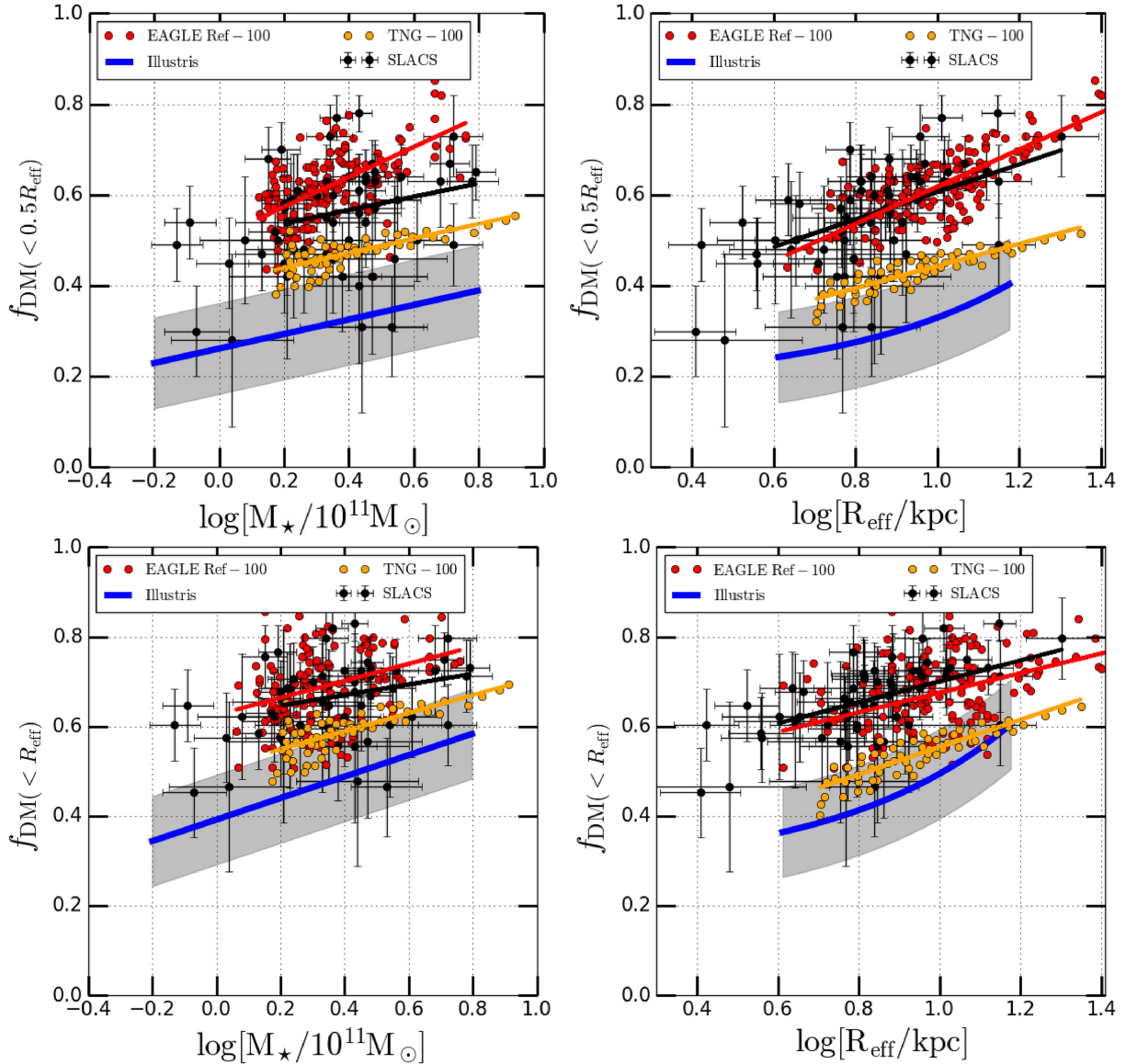


Figure 1. Top row: Comparison between the EAGLE Reference 100 cMpc simulation at $z = 0.271$ (red dots), Illustris (blue line) and IllustrisTNG (orange dots) at $z = 0.3$, and SLACS (black dots) for trends in $f_{\text{DM}}(< 0.5R_{\text{eff}})$ with stellar mass, M_{\star} (top left panel), and with effective radius (R_{eff}) (top right panel). Bottom row: Idem for $f_{\text{DM}}(< R_{\text{eff}})$. Both comparisons assume a constant stellar M/L ratio and a Chabrier IMF.

for Illustris (Vogelsberger et al. 2014) at $z_1 = 0.3$, and found values of $f_{\text{DM}}(< 0.5R_{\text{eff}})$ lower by a factor of 2–3 than SLACS.

However, the ratio of the projected dark-matter mass over the projected total mass can appear to be in good agreement even if both the projected stellar mass and the projected dark mass are incorrect. Thus, in Fig. 2 we also compare the sum of stellar and dark-matter masses inside $R_{\text{eff}}/2$ and R_{eff} to the total stellar mass. Also, in this case, we find that EAGLE agrees well with SLACS, whereas Illustris and TNG galaxies do not.

To further characterize EAGLE ETGs and understand the discrepancies with other simulations, we plot their size–mass relation in Fig. 3. We find that the EAGLE Ref-100 cMpc simulation yields ETGs with slightly larger effective radii compared to SLACS, about 0.1–0.2 dex at similar stellar masses. In M19, we discussed possible systematics that could explain this small difference. We also compare Ref-100 with non-lensing galaxies of Shen et al. (2003) and Baldry et al. (2012) and find good agreement. For IllustrisTNG,

the sizes are about 0.3 dex larger than those for SLACS and about 0.2 dex larger than the observations of Shen et al. (2003). The stellar mass–size relation of simulated EAGLE Ref-100 galaxies is slightly steeper than that for Illustris galaxies but shallower than IllustrisTNG galaxies (see also fig. 2 in Genel et al. 2018). Thus, we see that the difference in the size of a typical ETG between EAGLE, Illustris, and Illustris-TNG is a few kpc. On the other hand, the difference in dark-matter fraction is almost a factor of 2, which cannot be compensated with just the difference in their mass–size relation. Hence, these moderate mass–size relation differences are not the explanation for the lower dark-matter fractions in Illustris and IllustrisTNG.

Finally, in Fig. 4, we show the correlation between the total mass-density slope (γ) and $f_{\text{DM}}(< 0.5R_{\text{eff}})$ in EAGLE, IllustrisTNG, and SLACS. Although EAGLE Ref-100 and SLACS overlap, IllustrisTNG predicts a steep decrease in dark-matter fraction with γ that is not observed in SLACS.

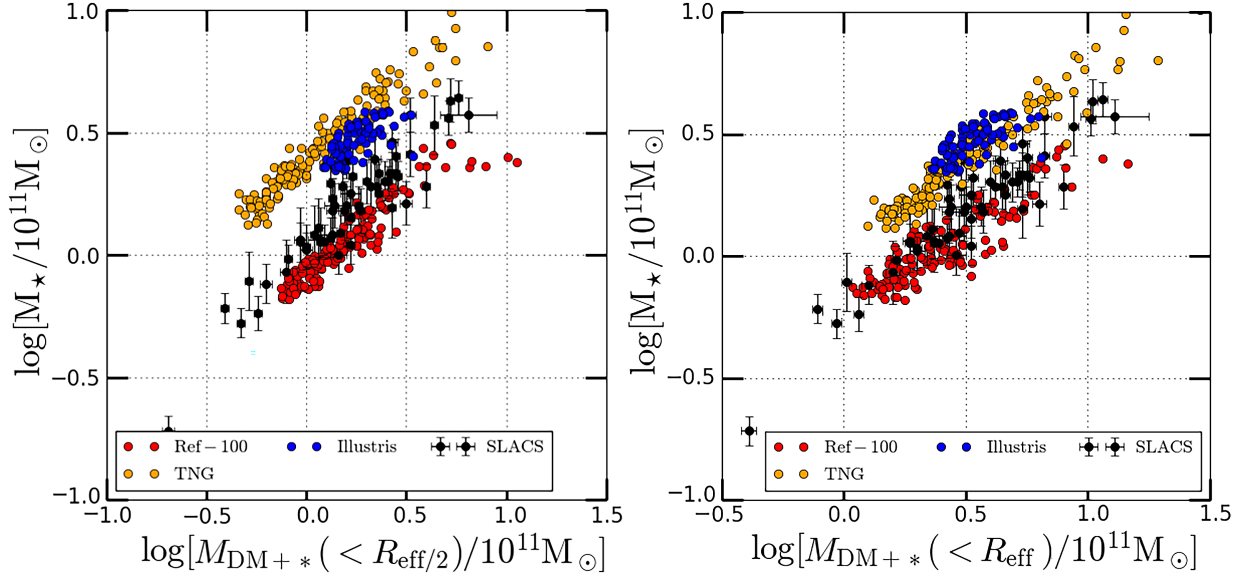


Figure 2. Comparison between the EAGLE Reference 100 cMpc simulation at $z = 0.271$ (red dots), Illustris (blue dots), TNG (orange dots) at $z = 0.3$, and SLACS (black dots) for trends in the combined stellar and dark-matter masses ($M_{\text{DM}+*}$) at $R_{\text{eff}}/2$ with total stellar mass, M_* (left-hand panel), and at R_{eff} (right-hand panel). Both comparisons assume a constant stellar M/L ratio and a Chabrier IMF.

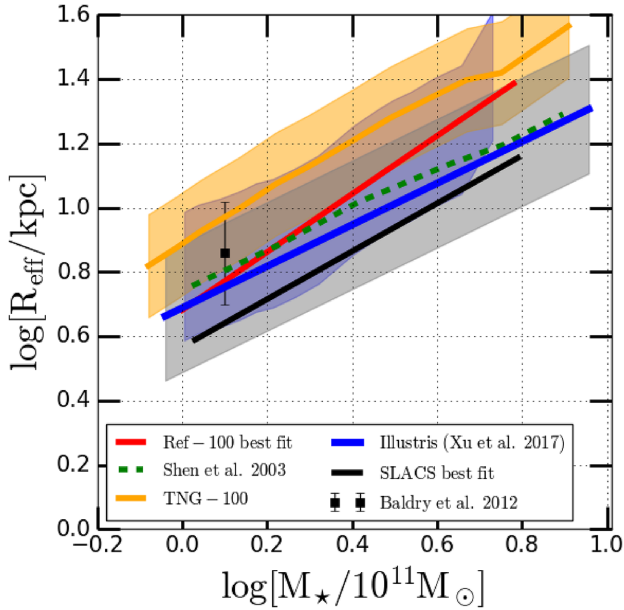


Figure 3. Comparison between the EAGLE Reference 100 cMpc simulation at $z = 0.271$ (red line), Illustris (blue line), and IllustrisTNG (orange line) at $z = 0.3$, and SLACS (black line) and other non-lensing studies for trends in effective radius (R_{eff}) with stellar mass (M_*). The shaded region is 2σ of each distribution. The overall distribution of EAGLE galaxies is shown as blue shaded region.

In a recent study, Remus et al. (2017) measured $f_{\text{DM}}(< R_{\text{eff}})$ from the MAGNETICUM PATHFINDER simulations (Hirschmann et al. 2014) and concluded that the dark-matter fractions are similar to observations of SLACS inside $R_{\text{eff}}/2$. However, comparing f_{DM} at these two different scales can lead to ≈ 30 – 40 per cent differences (Xu et al. 2017; Lovell et al. 2018). Remus et al. (2017) also did not reveal any clear correlation between stellar mass and central dark-matter fractions. This contrasts sharply with the clear correlation

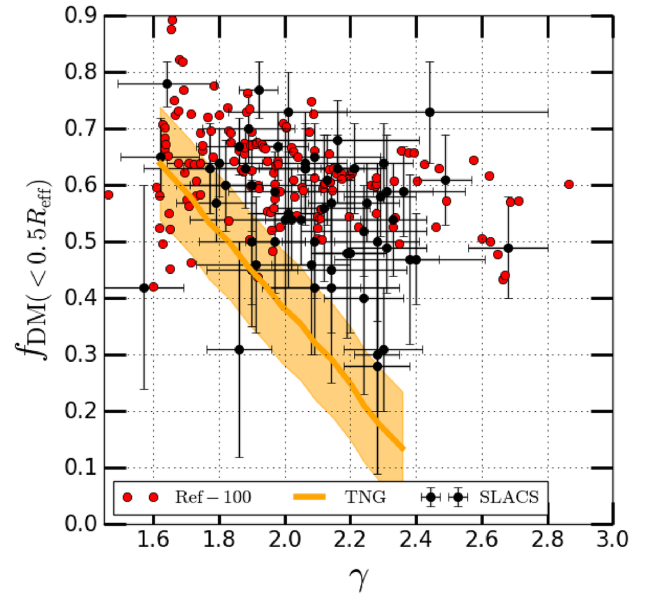


Figure 4. Comparison between the EAGLE Ref-100 (red dots), IllustrisTNG (orange line), and SLACS (black dots) for trends in $f_{\text{DM}}(< 0.5R_{\text{eff}})$ with γ . Illustris has lower DM fraction than IllustrisTNG; thus, its trend is not included here.

between those quantities in both the EAGLE Ref-100 simulation and SLACS (see the top panel of Fig. 1).

4.2 Dark-matter fractions inside R_{eff}

To test whether these discrepancies persist at larger radii, where finite resolution effects in the simulations are fractionally smaller, we examine the dark-matter fraction inside R_{eff} (see Section 3.2). In the bottom row of Fig. 1, we show the trends in $f_{\text{DM}}(< R_{\text{eff}})$ with stellar mass (bottom left panel) and effective radius (bottom right panel) for EAGLE Ref-100, Illustris, IllustrisTNG, and SLACS. Whereas

EAGLE Ref-100 again has an overall good agreement with SLACS, Illustris and IllustrisTNG have considerably lower dark-matter fractions. For increasing values of R_{eff} and M_* , though, the differences decrease. Even though the difference in dark-matter fraction between IllustrisTNG and SLACS has improved from $R_{\text{eff}}/2$ to R_{eff} , it is still lower than both SLACS and EAGLE by a factor of ≈ 1.5 .

5 DISCUSSIONS AND CONCLUSIONS

We have investigated the central projected dark-matter mass fraction inside half and full effective radii of simulated galaxies with stellar masses exceeding $10^{11} M_{\odot}$, (a) comparing the results to the mass-selected (strong-lens) galaxies from the SLACS survey, under the assumption of a universal Chabrier stellar IMF, and (b) investigating trends in the dark-matter fraction with galaxy mass, size, and mass-density slope for the EAGLE Ref-model, Illustris, and IllustrisTNG simulations. Our main conclusions are as follows:

(i) The dark-matter fractions inside $R_{\text{eff}}/2$ and R_{eff} found in EAGLE simulations are in good agreement with those inferred from observed SLACS galaxies. As one progresses to more massive and larger galaxies, the dark-matter fraction increases. This trend is also similar to that seen for strong-lensing observations in SLACS. EAGLE also reproduces the observed relation between dark-matter fraction and the slope of the total density profile.

(ii) Illustris and IllustrisTNG galaxies have lower dark-matter fractions than SLACS observations and EAGLE inside both $R_{\text{eff}}/2$ and R_{eff} . We attribute this difference to differences in the subgrid feedback models, which appears to lead to an overaccumulation of baryons in the inner central regions of galaxies in Illustris and IllustrisTNG.

The large differences in the dark-matter fractions between the Illustris and IllustrisTNG simulations and SLACS observations decrease, although do not disappear, when compared within one effective radius (see Remus et al. 2017; Lovell et al. 2018). The difference between the dark-matter fractions at R_{eff} and $R_{\text{eff}}/2$ is too large to be attributed purely to observational and numerical resolution effects. The significant differences between EAGLE and Illustris(TNG) simulations suggest that different, or additional, mechanisms controlling star formation processes and the (re)distribution of dark matter or stars play an important role in massive ETGs. The assumption of a universal (Chabrier) stellar IMF may be incorrect (Smith et al. 2015; van Dokkum et al. 2017); in fact, relaxing this assumption can lead to changes in the inferred dark-matter fraction with effective radius and galaxy mass (e.g. Tortora, Romanowsky & Napolitano 2013, and reference therein). Moreover, low-mass stars might be more prevalent at smaller radii, mimicking dark matter concentrated in the galaxy centres in the observations (e.g. Barber et al. 2018). However, our work suggests that we do not need to invoke a different IMF to resolve the mismatch in dark-matter fraction between simulations and observations. However, analysing if this can affect in some way the results of the paper is not possible. In fact, if from one side many works have analysed SLACS galaxies within a non-universal IMF scenario, simulations would require a self-consistent implementation of a variable IMF or an IMF different from the standard one. Also, this is not accounted for in all the analysed simulations, preventing us from a detailed comparison.

We will investigate the impact of different types of feedback mechanisms and a non-universal IMF on the dark-matter fraction in EAGLE galaxies in a forthcoming publication.

ACKNOWLEDGEMENTS

We thank the anonymous referee for her/his useful comments, suggestions, and helping us to improve the paper to its current form. SM and LVEK were supported through an NWO-VICI grant (project number 639.043.308). SM also acknowledges funding from COSMICLENs: ERC-2017-ADG, Grant agreement ID: 787886. RBM's research was supported by grant PRIN-MIUR 2017WSCC32. MS was supported by VENI grant 639.041.749. JS was supported by VICI grant 639.043.409. GV has received funding from the Marie Skłodowska-Curie grant agreement number 897124. SM thanks Fabio Bellagamba and D. D. Xu for useful discussions.

DATA AVAILABILITY

EAGLE simulation data are available at <http://icc.dur.ac.uk/Eagle/database.php>. Illustris and IllustrisTNG data are available at <http://www.illustris-project.org/> and <https://www.tng-project.org/data/>, respectively. Any other requests can be made to SM/LVEK.

REFERENCES

- Auger M. W. et al., 2009, *ApJ*, 705, 1099
 Auger M. W. et al., 2010a, *ApJ*, 721, L163
 Auger M. W. et al., 2010b, *ApJ*, 724, 511
 Baldry I. K. et al., 2012, *MNRAS*, 421, 621
 Barber C., Crain R. A., Schaye J., 2018, *MNRAS*, 479, 5448
 Barnabè M. et al., 2011, *MNRAS*, 415, 2215
 Bellagamba F., Tessore N., Metcalf R. B., 2017, *MNRAS*, 464, 4823
 Bolton A. S. et al., 2006, *ApJ*, 638, 703
 Cappellari M. et al., 2006, *MNRAS*, 366, 1126
 Chabrier G., 2003, *PASP*, 115, 763
 Cole S., Lacey C. G., Baugh C. M., Frenk C. S., 2000, *MNRAS*, 319, 168
 Crain R. A. et al., 2015, *MNRAS*, 450, 1937
 Dalla Vecchia C., Schaye J., 2012, *MNRAS*, 426, 140
 Dubois Y., Gavazzi R., Peirani S., Silk J., 2013, *MNRAS*, 433, 3297
 Duffy A. R. et al., 2010, *MNRAS*, 405, 2161
 Dutton A. A., Treu T., 2014, *MNRAS*, 438, 3594
 Gavazzi R. et al., 2007, *ApJ*, 667, 176
 Genel S. et al., 2018, *MNRAS*, 474, 3976
 Hirschmann M. et al., 2014, *MNRAS*, 442, 2304
 Humphrey P. J., Buote D. A., 2010, *MNRAS*, 403, 2143
 Koopmans L. V. E. et al., 2006, *ApJ*, 649, 599
 Koopmans L. V. E. et al., 2009, *ApJ*, 703, L51
 Li R. et al., 2019, *MNRAS*, 490, 2124
 Lovell M. R. et al., 2018, *MNRAS*, 481, 1950
 McAlpine S. et al., 2016, *Astron. Comput.*, 15, 72
 Metcalf R. B., Petkova M., 2014, *MNRAS*, 445, 1942
 Mukherjee S. et al., 2018, *MNRAS*, 479, 4108 (M18)
 Mukherjee S. et al., 2019, *MNRAS*, 504, 3455 (M19)
 Napolitano N. R., Romanowsky A. J., Tortora C., 2010, *MNRAS*, 405, 2351
 Nelson (2019) Computational Astrophysics and Cosmology, , 2197-7909
 Petkova M., Metcalf R. B., Giocoli C., 2014, *MNRAS*, 445, 1954
 Pillepich A. et al., 2018, *MNRAS*, 473, 4077
 Planck Collaboration XVI, 2014, *A&A*, 571, A16
 Remus R.-S. et al., 2017, *MNRAS*, 464, 3742
 Rosas-Guevara Y. M. et al., 2015, *MNRAS*, 454, 1038
 Salpeter E. E., 1955, *ApJ*, 121, 161
 Schaller M. et al., 2015, *MNRAS*, 451, 1247
 Schaye J. et al., 2015, *MNRAS*, 446, 521
 Schaye J., Dalla Vecchia C., 2008, *MNRAS*, 383, 1210
 Shen S., Mo H. J., White S. D. M., Blanton M. R., Kauffmann G., Voges W., Brinkmann J., Csabai I., 2003, *MNRAS*, 343, 978
 Shu Y. et al., 2017, *ApJ*, 851, 48
 Smith R. J. et al., 2015, *MNRAS*, 454, L71
 Springel V., 2005, *MNRAS*, 364, 1105

- Springel V., 2010, *MNRAS*, 401, 791
Tessore N., Bellagamba F., Metcalf R. B., 2016, *MNRAS*, 463, 3115
Thomas J. et al., 2011, *MNRAS*, 415, 545
Toomre A., Toomre J., 1972, *ApJ*, 178, 623
Tortora C. et al., 2009, *MNRAS*, 396, 1132
Tortora C. et al., 2012, *MNRAS*, 425, 577
Tortora C. et al., 2014, *MNRAS*, 445, 115
Tortora C. et al., 2018, *MNRAS*, 473, 969
Tortora C., Romanowsky A. J., Napolitano N. R., 2013, *ApJ*, 765, 8
Trayford J. W. et al., 2015, *MNRAS*, 452, 2879
Treu T. et al., 2006, *ApJ*, 640, 662
Treu T., Koopmans L. V. E., 2004, *ApJ*, 611, 739
van Dokkum P. et al., 2017, *ApJ*, 841, 68
Vogelsberger M. et al., 2014, *MNRAS*, 444, 1518
Wang Y. et al., 2019, *MNRAS*, 491, 5188
Wiersma R. P. C. et al., 2009b, *MNRAS*, 399, 574
Wiersma R. P. C., Schaye J., Smith B. D., 2009a, *MNRAS*, 393, 99
Xu D. et al., 2017, *MNRAS*, 469, 1824

This paper has been typeset from a $\text{\TeX}/\text{\LaTeX}$ file prepared by the author.